

Research Article

¹Department of Physics, McGill University, Montreal, QC, Canada

Keywords

Astrophysics, High-Energy, Pulsar, Gamma-Ray, *Fermi*-LAT

Email Correspondence

amanda.cook@mail.mcgill.ca

Exploration of *Fermi*-LAT Data: An Analysis of Pulsar J1930+1852

Abstract

Background: *Fermi*-LAT's 9-year data set of astrophysical gamma-rays (recently reprocessed) has revealed many new astrophysical sources. A closer analysis of one of these previously unseen sources, PSR J1930+1852 and associated pulsar wind nebula, G54.0+0.3, could help to confirm the gamma-ray emission mechanism of pulsars.

Methods: An investigation and analysis of PSR J1930+1852 and PWN G54.0+0.3 using *Fermi*-LAT data and science tools using maximum likelihood fitting is detailed.

Results: A 4.3σ ($p = 0.000017$) excess above background was observed at the coordinates of the pulsar/pulsar wind nebula and the sources spectrum appears to be consistent with a single power law.

Limitations: The sources in the models are modelled as point sources. Further studies may want to consider the possibility of extended sources in the modelled region.

Conclusion: There is evidence for a *Fermi*-LAT detection of this pulsar wind nebula and the source spectrum appears to be consistent with a standard power law. An upper limit calculation predicts only about 100 events with energy above 1 GeV in the 9-year data set so a pulsation search was not conducted.

Introduction

The Large Area Telescope (LAT) is a gamma-ray detector, one of the instruments on the *Fermi* satellite, specifically sensitive to photons in the energy range ~ 10 MeV to > 300 GeV where eV is electronvolt. Gamma rays that enter the detector are converted by tungsten foil to positron-electron pairs which are then tracked by silicon strip detectors. The telescope was launched in 2009 and by mid 2017 had detected over 200 million photon events. It orbits the earth every 96 minutes with the entire sky being surveyed in two orbits. The goal of this paper is to investigate very-high energy (VHE) astrophysical sources using publicly available *Fermi*-LAT data and Science Tools¹. Pulsars are one example of an astrophysical source which can emit in the VHE range. Pulsars are highly magnetized rotating stars (specifically neutron stars or white dwarfs) which emit beams of electromagnetic radiation which can be observed when the beam is pointing towards Earth, which happens every rotational period, hence the pulsed nature and the name of the stars. Pulsars have a magnetosphere, which is the region of space surrounding a source in which charged particles are controlled by the sources magnetic field.⁽⁶⁾ A pulsar wind nebula is a region of particles accelerated in a shock formed by the interaction between the pulsar's particle or magnetic flux and surrounding matter.⁽¹⁾

PSR J1930+1852 is young, energetic non third *Fermi*-LAT point source catalog (3FGL) ⁽²⁾² pulsar. The first evidence of the pulsar was seen in 2002 in radio and x-ray emissions,⁽⁷⁾ but its associated pulsar wind nebula G54.0+0.3 was observed in 1985.⁽⁸⁾ It has a characteristic age (approximate age based on the slowing of the rotation of the pulsar) of 2900 years.⁽⁷⁾ Both of these anomalous attributes are shared with the Crab pulsar, which has a characteristic age of 1257 years and emits in the VHE range.⁽⁹⁾ The Crab pulsar also has a rare broken power law spectral energy distribution (SED) as seen by VERITAS (Very Energetic Radiation Imaging Telescope Array System, a ground-based gamma-ray observatory) in 2011.⁽¹⁰⁾ Because of the other properties the Crab and PSR J1930+1852

share, the possibility of a broken power law SED in PSR J1930+1852 was investigated.

A source SED is the change of the flux with increasing energy, and a broken power law is one possible mathematical description of this relationship. In contrast to a standard power law in which the flux is proportional to the energy by some power or index, a broken power law has some cut off energy at which the SED has a different index, as illustrated below (Fig. 1).

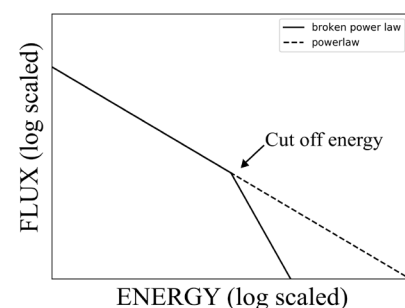


Fig. 1. An illustration of a spectrum in units of flux or plot of flux versus energy to illustrate the difference between a power law and a broken power law.

The detection of another pulsar with a broken power law in its VHE SED could add evidence for the mechanism for which pulsars are able to emit in the gamma-ray band. For example, there are models in which inverse Compton upscattering is the main emission mechanism which would be strongly supported by the detection of pulsars with broken power law spectra.⁽⁵⁾ The analysis of G54.1+0.3 SED is also interesting because current measurements by different instruments operating at higher energies are in disagreement;^(2,3) one of the goals was to better understand the SED behaviour across a broad energy spectrum. It has been seen by oth-

¹ Data and Science Tools are available at <https://fermi.gsfc.nasa.gov/ssc/data/access/>.

² The Third LAT Point Source Catalog, often abbreviated to 3FGL, is a catalog of over 3000 sources released by the LAT team after approximately 4 years of data taking.

er terrestrial detectors operating at higher energies, VERITAS (3) and HAWC (4) (High Altitude Water Cherenkov Observatory, a gamma-ray and cosmic ray observatory), but it was previously undetected in 9 years of *Fermi*-LAT data.

Methods

All *Fermi*-LAT photons from a 2.5-degree radius circular region near PSR J1930+1852 (specifically centred at our first estimation of its location based at right ascension 292.62 and declination +18.87) were selected and a model was made of the expected contribution from each source in the region. The model included possible emission from PSR J1930+1852; comparison with data was done via maximum likelihood estimation. Maximum likelihood estimation is a method of estimating parameters of a given model based on a sample population, done by maximizing the likelihood of making the observations in the sample given the parameters³. Here, the likelihood is the log of the probability assuming Poisson statistics in each energy bin in the SED. *Fermi*'s binned maximum likelihood function was utilized in the maximum likelihood fitting.

The steps of the fitting were to first make a data subselection around the region of interest and cut the data based on event class to ensure quality of the event data and zenith angle to discard non-astrophysical photons. The photon event files are from *Fermi* data version pass 8 between 239557417 s mission elapsed time (MET) and 518061255s MET. Next, one of the source model files (detailed below) was created from sources in the data region and up to 10° around it. Then the diffuse source responses were computed which depend on the instrument response function and finally the maximum likelihood fit was run. This final step was done twice, first to estimate the free parameters using a faster but less accurate optimizer (DRMNFB) and, from these estimates, apply a more accurate and CPU intensive optimizer (NEWMINUIT). DRMNFB finds the local minima of a continuously differentiable function subject to simple upper and lower bound constraints. NEWMINUIT is an interface to the C++ version of MINUIT, a well-known physics analysis tool for function minimization from CERN. This process was performed 3 times, once for each model. Test statistic maps, which search for unmodelled sources by calculating the likelihood of an additional source at each pixel of the map were made using another package in the Science Tools for the successful models. Finally, the upper limits of the flux from this source were computed assuming a power law model in Python (using *Fermi* Science Tools package). The other sources and their parameters were from 3FGL; all of the expected sources in the region and sources up to 10 degrees outside of the region were included, in case they contributed any photons as well. Three models were made; the first, shown in a counts map in the middle panel of the Fig. 2, is based on a model including only 3FGL sources, not the source of interest, PSR J1930+1852. The right panel of Fig. 2 is a model including all the 3FGL sources and a point source included for the pulsar with a fitted power-law spectrum. The equation for the power-law spectrum is

$$\frac{dN}{dE} = N_0 \left(\frac{E}{E_0} \right)^\gamma,$$

where N_0 is the prefactor, γ is the index, E_0 is the scale, and dN/dE is the integrated flux. The last model made was the same as the previously mentioned model except fitted with broken power-law source model. The equation for the broken power-law source model is

$$\frac{dN}{dE} = N_0 \times \begin{cases} (E/E_b)^{\gamma_1} & \text{if } E < E_b \\ (E/E_b)^{\gamma_2} & \text{otherwise} \end{cases},$$

where N_0 is the prefactor, E is the energy, E_b is the cut-off energy, dN/dE is the integrated flux, γ_1 is the index for energies less than the cut-off energy and γ_2 is the index for energies greater than the cut-off energy. The current *Fermi* galactic diffuse emission model and corresponding extragalactic isotropic diffuse emission were also accounted for and fit in all of these

models. These background models and the 3FGL sources were fit with free amplitude parameters to account for possible variation. Then the maximum likelihood program was run on each of these models which would fit the background models, fit the source parameters and obtain their resulting "test statistics". The test statistic value is a way to quantify the quality of the maximum likelihood fit, and it roughly represents σ^2 significance for a normal ("Gaussian") distribution - so a larger value implies a higher likelihood of a gamma-ray signal. The formula for the test statistic is

$$TS = -2 \ln \left(\frac{L_{max_0}}{L_{max_1}} \right),$$

where TS is the test statistic, L_{max_0} is the maximum likelihood value for a model without an additional source and L_{max_1} is the maximum likelihood value for a model with the additional source. Notice that the source of interest (just above and to the left of the center of the image) is far from being the brightest in the region.

Results

The precise results of the single power-law fit are as follows:

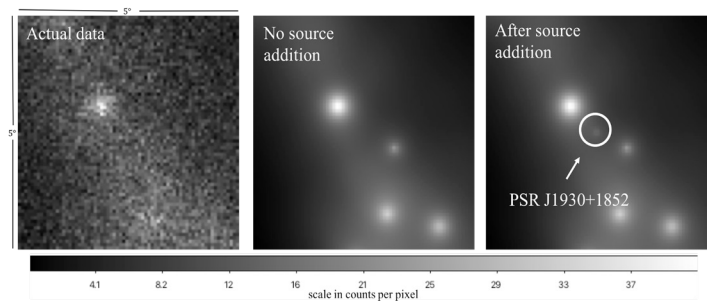


Fig. 2. Counts maps in the region of interest of (from left to right): *Fermi* data, the 3FGL point-source model without a new point source at the location of PSR J1930+1852 included, and the model with a source included (a power law pictured here, but a broken power law is visually the same). Each image is $5^\circ \times 5^\circ$.

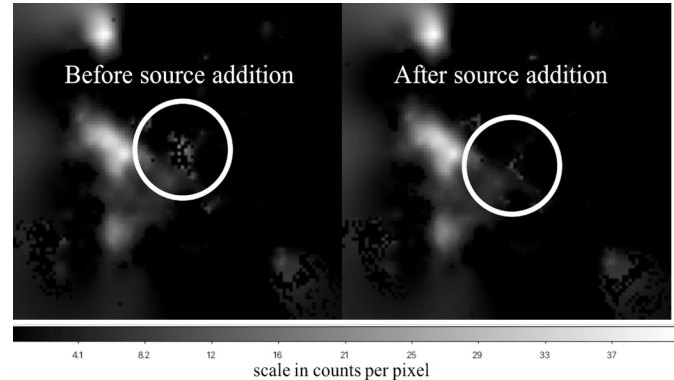


Fig. 3. Test Statistic map before and after adding to the model a source for PSR J1930+1852. Unexpected black pixels are likely due to the optimizer not converging in that pixel. If the model is an excellent fit to the data, one would expect the TS map to be close to featureless.

Prefactor (N_0): $0.03 \pm 0.03 \frac{\text{photons}}{\text{cm}^2 \text{s}}$

Index (γ): -1.9 ± 0.2

Scale (E_0): 100 MeV

TS value: 18.2 ($\sim 4.3\sigma$)

³ More information about maximum likelihood spectral fitting can be found on *Fermi*'s website, <https://fermi.gsfc.nasa.gov/ssc/data/analysis/documentation/Cicerone/Cicerone Likelihood/>.

Note: The uncertainty on the prefactor appears to be consistent with zero. However, the test statistic was used to assert the source inclusion; the large uncertainty is a product of the log scale used, i.e. it reflects accurately that the prefactor could be as great as 0.06 photons/cm²s. However, the range for values less than 0.03 photons/cm²s is smaller.

Discussion

Source Inclusion Justification

Evidence of a new source (not in the 3FGL (1) catalog) can be seen in the test statistic maps (Fig. 3), which justifies the inclusion of a source. The test statistic maps are a measure of the probability that there is a source in the particular pixel that is not accounted for in the model, i.e. the expected contributions are already subtracted. In pixels with high significance where there was not a source modelled, this is an indicator that there may be an unmodelled source present. It can be seen near the region of interest that there is an excess of high significance in the fit without the added source, which - given the relatively low brightness of the source - is especially in excess. However, as shown in the second plot (Fig. 3), once the source corresponding to PSR J1930+1852 is added and fit with free parameters the excess is reduced, signifying a better fit. Any unexpected single black pixels in the Test Statistic maps (Fig. 3) are likely due to the optimizer not converging in that pixel. In making these maps the maximum likelihood program is essentially run in every pixel and since convergence is not guaranteed some number of these black pixels are to be expected.

Spectral Model Justification

Next, to conclude that the *Fermi* data supports a power-law fit for this source and not a broken-power law for the SED, there were two main arguments based on the TS value. When this region was fit using the broken power law model the cut off energy would remain at the lowest energy bin reducing the spectrum to a standard power law. When forced to pick a different cut-off energy by only allowing its energy cut-off parameter to be fit in a range above the lowest energy, the program would return a fit with a negative test statistic for the source of interest. Since the test statistic roughly corresponds to the significance squared a negative test statistic value is unphysical in nature and thus a sign of a bad fit. However, when this region is fit with a power law for the SED, the optimizer would converge and a test statistic corresponding to the 4.3 σ observation was returned. The index of the successful model was -1.9 ± 0.2 , which is consistent with VERITAS reported index of SNR G54.1 + 0.3, $-2.39 \pm 0.30_{\text{sys}}$ from 100 GeV to above 30 TeV (3) but not consistent with HAWCs PSR J1930 + 1852 observation of an index of -2.74 ± 0.12 above 1 TeV.(4)

Upper Limit / Pulsed Signal

As this source is believed to be a pulsar, the next desired analysis was a pulsed signal search. A pulsed analysis was not done, however, because the upper limit flux calculation assuming the power-law model predicts the detection of only about 100 events from this source above 1 GeV in the entire 9-year *Fermi*-LAT data set. Although radio ephemerides⁶ exist for PSR J1930+1852, this number of events in the nine-year data set was too small to detect, in a statistically significant way, pulsed emission. However, this is an investigation that is worthwhile for future analysis. Without searching for a pulsed signal it cannot be stated whether the emission is from the pulsar or the associated pulsar wind nebula.

Conclusion

Strong evidence is presented for a *Fermi*-LAT detection of PSR J1930+1852 and its associated pulsar wind nebula GN54.1+0.3, previously unseen in *Fermi*'s data set. This source spectrum appears to be consistent with a single power law rather than the broken power law originally suspected. This contributes to the knowledge of the source SED and may help to resolve the current uncertainties. A limitation to this research is that all sources modelled were considered as point sources. Although the high significance suggests that this is a good approximation, for completeness and

further analysis, models including 3FGL extended sources in the region would be accounted for.

Another obvious extension of this research would be to search for a pulsed signal. However, given that an upper limit of the flux predicts approximately 100 events expected in the full 9-year data set, if pulsations were detected in this data after folding the data using an ephemeris derived from radio observations that is valid for the duration of the *Fermi* mission, it would likely be weakly. This can be considered as one of the drawbacks to the all-sky views that *Fermi*-LAT produces. If further research were to be conducted on this source, it would be recommended to use a more sensitive instrument with a deeper exposure, search this data for a pulsed signal, and use this combined with a pulsed radio detection to derive information about the magnetosphere of the pulsar.

Acknowledgements

I would like to thank my supervisors Prof. Ken Ragan and Dr. Ben Zitzer for their support, inspiration and mentorship.

I would also like to thank the NSERC URSA program for providing the funding for this research, and the McGill Physics Department for providing a nurturing environment.

References

1. H. An, K. Madsen, S. Reynolds, V. Kaspi, F. Harrison et. al. High-Energy X-Ray Imaging of the Pulsar Wind Nebula MSH 15-52: Constraints on Particle Acceleration and Transport. *Astrophys. J.* 2014 Oct 1; 793(1):90
2. F. Acero, M. Ackermann, M. Ajello, A. Albert, W. B. Atwood et. al. Fermi Large Area Telescope Third Source Catalog. *Astrophys. J. Suppl.* 2015 Jun 22; 218(2):23
3. V. A. Acciari, E. Aliu, T. Arlen, T. Aune, M. Bautista et. al. Discovery of Very High Energy γ -ray Emission from the SNR G54.1+0.3. *Astrophys. J. Let.* 2010 Jul 22; 719(1):L69
4. A. U. Abeysekera, A. Albert, R. Alfaro, C. Alvarez, J. D. A. Ivarez et. al. The 2HWC HAWC Observatory Gamma-Ray Catalog. *Astrophys. J.* 2017 Jun 29; 843(1):40
5. Lyutikov, M. and Otte, N. and McCann, A. et. al. The Very High Energy Emission from Pulsars: A Case for Inverse Compton Scattering. *Astrophys. J.* 2012 Jul; 754(1):30
6. Anatoly Spitkovsky Pulsar Magnetosphere: The Incredible Machine. *AIP Conference Proceedings* 2008 Jul; 983(1):20-28
7. F. Camilo, D. R. Lorimer, N. D. R. Bhat, E. V. Gotthelf, J. P. Halpern, et. al. Discovery of a 136 Millisecond Radio and X-Ray Pulsar in Supernova Remnant G54.1+0.3. *Astrophys. J.* 2002 Jul 20; (1)71-74
8. Reich, W., Fuerst, E., Altenhoff, W.J., Reich, P., Junkes, N, et. al. Evidence for two young galactic supernova remnants. *Astronomy and Astrophysics* 1985 Oct; 151(1)10-12
9. Na Wang et. al. A Large Glitch in the Crab Pulsar. *Chin. J. Astron. Astrophys.* 2001 Apr; 1(3)95-199
10. A. McCann. Detection of the Crab Pulsar with VERITAS above 100 GeV. *ICRC Proceedings* 2011 Oct 19; 32(1)